Dountcheva, I.; Sanz, D.; Cassiraga, EF.; Galabov, V.; Gómez-Alday, JJ. (2020). Identifying non-stationary and long-term river-aquifer interactions as a response to large climatic patterns and anthropogenic pressures using wavelet analysis (Mancha Oriental Aquifer, Spain). Hydrological Processes. 34(25):5134-5145. https://doi.org/10.1002/hyp.13934

Identifying non-stationary and long-term river–aquifer interactions as a response to large climatic patterns and anthropogenic pressures using wavelet analysis (Mancha Oriental Aquifer, Spain)

Running title: Identifying long-term river–aquifer interactions using wavelets

Names of authors

Iordanka Dountcheva[1], David Sanz[1], Eduardo Cassiraga[2], Vassil Galabov[3], Juan José Gómez-Alday[1].

Affiliation

[1]Hydrogeology Group, University of Castile–La Mancha, Albacete, Spain

[2]Hydraulics and Environmental Engineering Department, Polytechnic University of Valencia, Spain

[3]Technical University of Sofia, Bulgaria

Corresponding author: Iordanka Dountcheva

Corresponding author e-mail: iordanka.guenova@alu.uclm.es

Corresponding author address:

Hydrogeology Group**,** Institute for Regional Development

University of Castilla-La Mancha

Campus Universitario, s/n

02071 Albacete

Spain

Acknowledgements

Special thanks go to the Júcar Water Authority (CHJ) and stakeholders (JCRMO) in the Mancha Oriental System for providing the necessary information. The content of this report does not represent the view of CHJ and JCRMO.

This work has been funded by the research projects CGL2017-87216-C4-2-R from the National Research Program I+D+i (FEDER/Ministerio de Ciencia, Investigación y Universidades) and SBPLY/17/180501/000296 from the National Research Program I+D+i of the Junta of Communities of Castile–La Mancha.

We would also like to thank Christine Laurin for the English copy editing and valued comments.

Abstract

The objective of this study was to analyse periodicities and the long-term variability of monthly Júcar River–Mancha Oriental Aquifer interactions (RAI) and regionally measured precipitation (PP) with special focus on the correlations between these local hydrological variables and the large climatic patterns governing the Iberian Peninsula, represented by their teleconnection indices — the North Atlantic Oscillation (NAOi) and the Western Mediterranean Oscillation (WeMOi). To that end, wavelet analysis has been applied since it not only provides insight into the time series dynamics, but also permits statistical interpretation and correlation analysis. As a result, several periodicities have been detected: intermittent semi-annual periodicity in PP and the NAOi, and annual periodicity in the RAI, NAOi, and WeMOi time series. Long cycles (approximately 14 years) are also observed in the PP and WeMOi time series. The cross-wavelet spectra show a correlation between the RAI and the rest of the variables on the semi-annual and the annual scales, while wavelet coherence detects common behaviour with longer cycles — 5–6 years between the NAOi and the RAI, and cycles of both 1–5 years and 7–10 years between PP and the RAI. Furthermore, results show that the periodicities in the teleconnection indices and precipitation propagate into the RAI with certain lead times: 3 months between the RAI and PP and 6 months between the RAI and the NAOi. The results indicate that the detected periodicities and the coherence between the studied variables could have applications in strategic planning on a river basin scale, taking into account the propagation times and the frequency scale. This methodological approach can be applied into strategic water resource planning independently of the geographical location of the hydrogeological system, the basin size, and the climate region.

Keywords: River-Aquifer Interactions, Exchange Processes, Intensive Groundwater Use, Water Resource Planning, Wavelet Analysis, Long-term Variability, North Atlantic Oscillation, Western Mediterranean Oscillation

1. Introduction

Generally speaking, the planning and management of water resources is based on two premises: supply (reserves and resources) and demand (quantity and quality for different water uses). In the face of the continuous growth in demand in many parts of the world (see, among many other examples, the High Plains aquifer in the USA (Butler et al., 2018), groundwater systems of the Indian subcontinent (Mukherjee et al., 2015), and the Nubian aquifer in Africa (Puri & Aureli, 2009), some countries or unions of states (e.g. the European Union) have seen the need to take measures to protect the good status of water bodies and thus guarantee sustainability. The EU's Water Framework Directive (CEC, 2000), for instance, has established homogeneous environmental objectives among the states, highlighting the protection of ecosystems, hydrological planning, and management of river basins or hydrogeological systems. The planning envisages 6-year cycles and describes various types of activities undertaken in parallel throughout the entire process (hydrological plan, public consultations, the preparation and adjustments to the Program of Measures, and the process of strategic environmental assessment (https://www.miteco.gob.es/es/agua/temas/planificacion-hidrologica/planificacion-hidrologica/nuevo-proceso-planificacion/). Hydrological planning methods and techniques assume stationarity of the hydrological regime. However, Milly et al. (2008, and references therein), indicate that stationarity should no longer serve as the central assumption in the evaluation and planning of water resources, largely due to the natural variability of low-frequency climate oscillations and global warming. In addition, non-linearity increases in the case of river basins or hydrogeological systems formed by large aquifers, with complex relationships with superficial resources, and under anthropogenic pressures that can modify system behaviour. In effect, both the evolution of system resources estimated from climatic and hydrological variables and the evolution of demands (pressures and environmental needs) are stochastic and non-stationary variables in behaviour, and present many scales of variation in time and frequency (Grinsted et al., 2004; Maraun & Kurths, 2004). Consequently, methods that can identify localized intermittent periodicities are required for these types of studies (Boggess et al., 2009). Appropriate analytical methods are needed so that the analysis of hydrological time series takes into account non-stationarity in hydro-climatic processes and its analysis can be projected to planning cycles.

Wavelet analysis techniques are widely used for time series analyses of different natures — geophysical, hydrological, meteorological, human metrics and heart rates, internet traffic, and many others. These techniques are also chosen to study the long-term behaviour of climatic variables since

they do not make assumptions of stationarity or linearity (Grinsted et al., 2004; Markovic & Koch 2013; Torrence & Compo 1998). Wavelet analysis consists in decomposing a process into arbitrarily chosen wavelet functions and provides information about the time series for different frequency scales and time intervals (Daubechies, 1992). Furthermore, cross-wavelet spectra and wavelet coherence could provide a better understanding of the relations between climatic and hydrogeological variables. Some studies have applied these techniques for aquifers and hydrogeological systems (Andreo et al., 2006; Charlier et al., 2015; Holman et al., 2011; Komasi & Shargi 2019; Labat et al., 2001; Sang Y-F et al., 2012, among others). However, to our knowledge, this methodology has not been applied to analysing river-aquifer interactions under anthropogenic pressure (intensive groundwater use) and its relations with the large climate patterns represented by their teleconnection indices and precipitation (as drivers for groundwater recharge).

This study focuses on one of the most extensive and exploited carbonate hydrogeological aquifer systems in Europe with complex relations between groundwater (the Mancha Oriental Aquifer) and surface water (the Júcar River). The objective is to use wavelet analysis to investigate the long-term variability of regionally modelled river-aquifer interactions and their links to large-scale teleconnection patterns and precipitation in order to identify changes both in periodicity (time and frequency domain) and system behaviour that are not detectable by traditional statistical methods. Therefore, this study may provide a significant contribution to establishing more precise ways to plan cycles and/or specific water management measures in hydrogeological systems like the Mancha Oriental Aquifer, based on observed hydrogeological variables.

2. Study Area

The Júcar River Basin (JRB) (surface area of 42,735 km^2) is located in the southeastern Iberian Peninsula and comprises various watersheds that flow into the Mediterranean Sea. From a strategic point of view, the JRB has three main areas related to water resource demand and drought management: (a) the upper inland areas, where river water is stored in reservoirs; (b) the mid-basin inland areas, with significant groundwater storage and where the aquifer-river interactions take place; and (c) the coastal areas, the location of the major water demands (Figure 1). According to recent studies (Gómez-Martínez et al., 2018) on a river basin scale the total annual stream flows are estimated at 3,343.8 hm^3 - 33% account for surface water, while 67% represent groundwater base flow to the river network, of which 32% contributes to the wetlands and the Mediterranean sea.

This study is focused on the mid-basin inland area with practically flat topography (700 metres above sea level), interrupted only by the valley carved out by the Júcar River. The area has a semi-arid continental climate with extreme temperatures in both winter and summer, with monthly temperatures averaging 6°C in winter and 22°C in summer. These climatic conditions are determined by the elevation and the geographical location on the edge where the Atlantic and the Mediterranean climatic influences take place (Martin-Vide & Lopez-Bustins, 2006). The precipitation is associated with the predominant effect of the Atlantic fronts, combined with the local affluence of the Mediterranean sea. Mean values are about 350 mm/year, varying from 280 mm/year, at the southern boundary, to 550 mm/year, in the northern zone. The potential evapotranspiration of a reference crop (*Festuca arundinacea*) is approximately 1,200 mm/year.

At the head of the mid-basin, one of the JRB's largest reservoirs (the Alarcón reservoir, 1,118 hm^3) was built in the mid-1940s in order to regulate the Júcar River flow. This river flow produces hydroelectrical power and supply water to: (a) irrigated croplands in the Valencia plain (approximately 470 km^2 with some 60,000 farmers in the Júcar-Turia and La Acequia Real del Júcar irrigation systems), (b) the populations of Albacete and Valencia cities (170,000 and 1,000,000 inhabitants, respectively), and (c) the Albufera wetlands, important for rice farming, tourism, and fishing.

In addition to the Alarcón reservoir control, the Júcar River flows in the mid-basin are heavily influenced by complex hydrogeologic relations with the Mancha Oriental Aquifer (MOA). The MOA with 7,260 km^2 in extent comprises one of the largest carbonate aquifers in Spain. This multi-layered karstic system is formed by the superposition of nine hydrological units, where the Middle Jurassic, Upper Cretaceous, and middle Miocene aquifers are separated by semipermeable materials that act as aquitards. The impermeable bottom of the system includes the marls, clays, and gypsum of the Lower Jurassic (and, sometimes, Triassic). A complete description of the aquifer and the conceptual model constructed for its understanding can be found in Sanz et al. (2009).

Under natural (non-human influenced) conditions, the Júcar River would be the main recipient of groundwater discharge for the MOA (Figure 1). MOA available resources are estimated at 359.7 hm^3/year (CHJ 2015) and are derived from precipitation infiltration, lateral groundwater inflow, irrigation excess, infiltration from the Jardín and Lezuza rivers and wastewater from the city of Albacete. Starting in the mid-1970s, approximately 1,000 km^2 of irrigated lands became dependent on groundwater (Figure 1), which allowed for significant socioeconomic growth in the area. Currently, approximately 320.0 hm^3 of groundwater are pumped per year, of which 98% is used for

agriculture. According to the Júcar River Basin Management Plan (CHJ 2015), the volume of groundwater withdrawals exceeds that of the available recharge, which is estimated at 275,3 hm^3/year. The intensive exploitation of groundwater coupled with droughts, such as that in the early 1990s (1990–1994), have led to significant decreases in piezometric levels and the volume of stored groundwater (Sanz et al., 2018). The preferential direction of the groundwater flow in the transient state changed in the mid-1990s from Júcar River as main discharge zone (gaining river) towards the cones of depression produced by pumping, converting it into a losing river in some reaches (Castaño et al., 2013).

Figure 1 near here.

3. Material

3.1. Climate Index Data

The large climate patterns governing the Iberian Peninsula and the Júcar River Basin are the North Atlantic Oscillation (NAO) and the West Mediterranean Oscillation (WeMO), represented by their monthly teleconnection indices — NAOi (dimensionless) and WeMOi (dimensionless) (Gómez-Martínez et al., 2018; López et al., 2010).

The NAO is a well-known pattern of the Earth's climate system with significant implications for the entire North Atlantic region. The NAOi is characterized by positive and negative phases and varies at inter-seasonal, inter-annual, and inter-decadal time scales (Hurrel 1995, Hurrell et al., 2003, Jones et al., 1997). Positive NAO phases are associated with cooler and drier conditions in southern Europe, the Mediterranean, and Greenland; in contrast, positive phases result in above-normal temperatures and precipitation in the eastern United States and across northern Europe. The opposite occurs during strong negative NAO phases (Jones et al., 1999; Osborn 2006).

Due to a relatively weak relationship between the precipitation of the eastern Mediterranean coastline of the Iberian Peninsula and the NAOi, a local mode of atmospheric circulation pattern called the West Mediterranean Oscillation (WeMO) was defined in an aim to improve our understanding of the climate drivers governing the torrential events typical of this region (Martin-Vide & Lopez-Bustins, 2006). Further studies show that, for the Gulf of Valencia, the WeMOi correlates better than the NAOi with monthly precipitation anomalies during autumn and winter; therefore, the index can be useful to forecast torrential rainfall events in the eastern part of the Iberian Peninsula (Lopez-Bustins et al., 2008).

3.2 Precipitation Data

As pointed out by Sanz (2005), significant meteorological pulses affect the entire MOA equally, basing his reasoning on the region's marked continentality. In general, small variations are conditioned by orography, so a comparison of the precipitation data from the stations chosen to perform wavelet analysis is consistent with that fact. The available precipitation time series (PP) have missing data, and so the moving average technique of interpolation has been used in order to reconstruct them. Furthermore, the precipitation time series from the three meteorological stations have been blended (see Figure 1 for the geographical position of each station). The descriptive statistics were obtained from the interpolated series (see results in Table 1).

Table 1 near here.

3.3 River-Aquifer Interactions

The river-aquifer interactions can be established using different methods (see a brief theoretical summary of the river-aquifer interaction in Osman & Bruen, 2002). However, spatial and temporal assessment, quantification, and prediction are generally performed using numerical models because of their ability to represent the complexity of hydrogeological systems (Fleckenstein et al., 2006).

To investigate the Júcar River and Mancha Oriental Aquifer interactions (RAI) under the exploitation of groundwater resources for irrigation, a numerical groundwater flow model was built. The study area was horizontally divided into three dimensions in 1 km^2 cells, aligned in a northerly direction, with 126 columns and 131 rows for a total of 16,506 cells per layer. Temporal discretization was defined for a period of 73 years (from 1940 to 2012), with periods of stress taken on a monthly basis. To simulate groundwater flow, the Modflow code was used (Harbaugh, 2005) in the graphical user interface ModelMuse (Winston, 2009). This interface solves the flow equation in a porous medium in three dimensions using an approximation by finite differences. The code consists of a main module and a large number of independent subroutines. These subroutines were grouped into packages that refer to particular aspects of the simulation. In this case, the packages used refer to: (a) external action wells (WEL), (b) recharge (RCH), and (c) conditions of internal contour rivers (RIV). The input data are the aquifer's hydraulic parameters, the boundary conditions, and the initial conditions. The model output is the piezometric head and the flow in each cell of the model, as well as the water budget (i.e. river-aquifer interactions). The model was considered calibrated and validated satisfactorily when the simulated and observed trends of groundwater evolution distributed spatially throughout the aquifer coincided. The full development of the model can be reviewed in Sanz et al.

(2011) and Cassiraga et al. (2013). For our purpose, the temporal series of river-aquifer interactions were obtained (Figure 2).

Figure 2 near here.

4. Methodology

4.1. Wavelet Transforms and Wavelet Spectra

Wavelet analysis provides insight into the dynamics of a process in both the time and the frequency domains. The wavelet transform is a suitable tool for the analysis of time series when no previous assumption for stationarity or linearity has been made, and when the focus is on low-frequency events. Furthermore, cross-wavelet transform and wavelet coherence can be calculated for a pair of time series. While the cross-wavelet spectra reveal high common power (correlation), the wavelet coherence finds common local phase behavior (covariation). The use of both provides a more comprehensive understanding of the relations existing between the two variables and the underlying physical processes.

A continuous wavelet transform of a discrete signal or a time series X_t for a constant interval of discretization Δt and t=0,1,…..T-1 is defined as:

$$W_X(s,u) = \sum_{t=0}^{T-1} X_t \, \psi^*_{s,u}(t), \quad (1)$$

and where

$$\psi_{su}(t) = \sqrt{\frac{\Delta t}{s}}\psi\left(\frac{(t-u)\Delta t}{s}\right) \quad (2)$$

The parameters $s \in R/0$ (dilation) and $u \in R$ (translation) are used to transform the so-called mother wavelet (2) into a family of wavelet functions. The symbol (*) denotes a complex conjunction.The global wavelet spectrum of X_t is given with the expression:

$$\|W_X(s,u)\|^2 = \frac{1}{T}\sum_{k=0}^{T-1}|W_X(s,u)|^2, \quad (3)$$

where k is the time index.

In this study, the Morlet wavelet is used with the following formula: $\psi(t) = \pi^{-1/4} e^{i\omega_0 t} e^{-t/2}$,

where ω_0 denotes the frequency. This wavelet mother function is very commonly used to analyse geophysical time series (Torrence & Compo 1997; Grinsted et al., 2004) because it provides a good compromise between frequency and time resolution. Errors occur due to the finite nature of the time series at the edges of the wavelet spectrum. In order to correctly consider these errors, the cone of influence is defined. It represents the time-frequency zone where these errors in the coefficients are negligible and, for the Morlet wavelet, it is where $u \leq \sqrt{2}s$ for each scale.

4.2. Cross-Wavelet Spectrum and Wavelet Coherence

Cross-wavelet spectrum and wavelet coherence provide an additional understanding and statistical interpretation, when two time series X_t and Y_t with wavelet transforms W_X and W_Y are compared. In such a case, the cross wavelet transform is defined as:

$$W_{XY}(s,u) = W_X(s,u)W_Y^*(s,u). \quad (4)$$

The cross-wavelet power is calculated as $|W_{XY}|$ and the shift between the two series is the arctg(W_{XY}), which can be interpreted as the lag between the two processes X and Y. Furthermore, normalization of the wavelet spectrum provides the wavelet coherence, which could be interpreted as the normalized covariance between the two time series X_t and Y_t.

4.3. Statistical Significance Tests

The statistical significance of the wavelet spectrum was tested assuming the null hypothesis that the time series are generated with red noise (*RedNoise*) autocorrelation properties. For each frequency scale and time series, the significant cycles were tested comparing their global wavelet spectrum to the spectrum of the red noise process. The *RedNoise* spectrum is approximated with a first-order autoregressive process. The spectrum coefficients were calculated following the formula $(\phi_1 + \phi_2^{0.5})/2$, where ϕ_1 and ϕ_2 are the lag 1 and 2 correlations of the corresponding time series. Monte Carlo simulations are used to test the statistical significance of the wavelet coherence. No coherence null hypothesis between the two time series was assumed. Matlab codes available from (Grinsted et al., 2004) have been used for the wavelet, cross-wavelet, and wavelet coherence analyses.

5. Results

Wavelet spectra analyses have been carried out first on all four data sets. The wavelet spectra plots of the studied variables are shown in Figure 3. Several frequency components were detected at the 95% significance level for all variables. The NAOi and PP display semi-annual and annual periodicity

above *RedNoise* intermittently for the entire study interval, whereas for the WeMOi the predominant periodicity is annual with attenuating power. On the RAI plot, there is a significant change in system behaviour from the 1980s on due to intensive Mancha Oriental aquifer withdrawals for irrigation. Prior to this year, 3-month cycles are detected. 4–5 year periodicity above *RedNoise* is present in all variables except the RAI, although it varies over time and for the NAOi it does not fulfill the statistical test. A 10-year periodicity is the only low frequency above *RedNoise* in the NAOi spectra plot detected in the early 1990s. The 12–14 year period is detectable in all variables for the entire study period, but surpasses the significance level only for precipitation. PP spectra have an 11–14 year cycle in the time window of 1950–1980 and, for the WeMOi, 12 and 14–20 year cycles are present for the entire study period within the cone of influence (COI), but only the latter is above *RedNoise*.

Figure 3 near here.

To find a correlation between the NAOi and WeMOi as climate drivers for PP and RAI, cross-wavelet spectrum analysis was performed. The plots of the corresponding cross-wavelet spectra are shown in Figure 4 a, b, c, d, and e. The time series of the NAOi and PP have common high power intermittently for the semi-annual period for most of the observed time window, whereas for the WeMOi and PP, this relation is weaker and detectable at both the semi- and the annual frequency scales. As refers to periodicities with lower frequencies in the cross-wavelet spectra between the two teleconnection indices and PP (Figure 4a and 4b, respectively), the biannual (2-year) component is above the *RedNoise* for both indices in the mid-1950s and for only NAOi in the mid-2000s. The 6–8 year frequencies are significant on the PP-NAOi plot in the 1998–2002 time window with a related 130-degree lag, corresponding to approximately 30 months NAOi lead. A 12-year cycle is present in the cross spectra PP-NAOi, and passes the statistical test from 1944 to 1954, whereas for the PP-WeMOi the frequency scales cover a 12–20 year period. The WeMOi leads PP by 90 degrees (approximately 45-month lag) from 1970 on.

The cross-wavelet spectra of the RAI series have areas of common power with the NAOi, WeMOi, and PP on the semi-annual and annual frequency scales. No other significant cycles are observed. A semi-annual cycle is detected in small intervals from 1985 to 2000 on the RAI-NAOi plots, whereas for the RAI-WeMOi relation, these time intervals are even shorter, starting at the beginning of the 1990s, and ending in the mid-2000s. The semi-annual periodicity is best represented on the RAI-PP cross-wavelet spectra, especially in the time window of 1985–1992. Note that, in all areas with a high common power, the two variables are in anti-phase, which corresponds to a 3-month lag between them.

A common power is detected above *RedNoise* on the annual cycle from 1985 on for all cross-wavelet spectra outputs (Figure 4 c-e). The RAI and NAOi are in anti-phase on the annual scale in the significant areas, which corresponds to a 6-month lag between them, whereas the RAI and WeMOi switch from anti-phase in the late 1980s to in-phase in the 1990s and then again to anti-phase from the mid-2000s until the end of the study period.

Figure 4 near here.

A wavelet coherence analysis was also performed in order to study the variables' dynamics and their localized correlation. Outputs are the graphics shown in Figure 4 (f, g, h, i, j). The wavelet coherence between the chosen teleconnection indices and PP is significant at the semi-annual scale intermittently for the entire study interval (Figure 4 f-g). On the other hand, wavelet coherence between the RAI and the rest of the variables is predominantly annual in scale (Figure 4h-j). The wavelet coherences PP–NAOi and PP–WeMOi display areas of significant common behaviour at the 5-year frequency scale in reduced time windows, which vary over time and at the 10-year frequency scale from 1984 on. Small and intermittent areas of common behaviour are detected on both graphic outputs for the annual frequency. No other periodicities with lower frequencies are significant in the RAI-WeMOi plots, whereas the RAI-NAOi has a correlation in the 3-year periodicity in the 1970s, where the NAO leads the RAI by approximately 20 months. Another periodicity that passes the statistical test is the 6-year one in the time window between 1950 and 1970, in which the NAO leads the RAI by approximately three years.

In the wavelet coherence plot between the PP and the RAI, there is semi-annual frequency with detectable common cyclical behaviour and few interruptions across the entire time interval. In that interval, the two variables are in anti-phase, which corresponds to three months of lag between them. A strong correlation is detected between the two variables, especially between 1945 and 1975 on the 1–5 year scales and on the 2–6 year scales between 1985 and 2000 with a constant delay of 135 degrees between PP and RAI. Another important periodicity (where the variables fulfill the statistical test) is detected on the 7–10 year scale in the time window of 1952–1978.

6. Discussion

The non-stationary analysis of the hydro-climatological variables that control the status of river basins or hydrogeological systems is crucial to carrying out proper planning and management of water resources. Several studies have used the wavelet methodology to better understand hydrogeological dynamics (Salerno & Tartari 2009; Holman et al., 2011), but none have analysed complex river-

aquifer relationships (obtained through simulation models) and their correlation with large-scale teleconnection patterns and precipitation under anthropogenic pressures. Even when a detailed knowledge of the hydrogeological behaviour of river-aquifer systems is available by means of numerical models, it is still necessary to establish the non-linear and non-stationary characteristics of the hydrogeological and climate variables involved. It could allow the timely identification of hydrological events with certain periodicities that are characterized by their intensity. In this regard, there are important periodicities or cycles for management purposes such as the time lag between precipitation and groundwater discharge to the river as well as their variability with respect to the climatological patterns of the area. This information is crucial for the planning and management processes of river basins, for instance, with drought management.

Hydrogeological knowledge of the MOA (Sanz et al., 2009; 2011) has allowed us to establish that the main variables that govern water management policies here are groundwater recharge by rain infiltration and river-aquifer interactions. River-aquifer interactions (RAI) shifted in the 1980s, with the beginning of intensive groundwater withdrawals for irrigation (Figure 2, 3). Indeed, since 1980 there has been a falling trend of groundwater contributions to the Júcar River flow, which introduces a non-stationary element in the RAI. Despite this non-linearity introduced by anthropogenic pressure, significant correlations have been detected with wavelet methodology between the RAI and climatological variables (NAOi, WeMOi, and PP).

An important result is the phase difference of 3 months between PP and RAI found from the wavelet coherence at the semi-annual frequency scale. It can be explained by delaying processes due to the transit time of precipitation infiltration across the unsaturated zone, which are in agreement with the residence times found by Sanz et al. (2011). Interestingly, for the longer periods of 1-5 and 2-6 years, the lead-time is also longer (around 16 months at the 4-year frequency). Furthermore, in the 1950-1970s, the phase difference at the frequency of 8 years is very similar – approximately 15 months (Figure 4j). This behaviour might suggest that groundwater movement and storage is increased when long-term fluctuations in PP and RAI occur. The effect on greater aquifer storage may be related to the non-linearity of the precipitation infiltration versus groundwater recharge. Remarkably, these frequencies, linked to natural recharge rates are not well detectable after 1975s when intensive MOA exploitation starts (Figure 4j). Indeed, after 1985 the annual periodicity (detected with the cross wavelet spectra) is significant, conditioned by seasonal river control and intensive aquifer exploitation, prevailing above the region´s climatic conditions (see Figure 2d and Figure 4c,d,e).

In the study area, it is worth noting that, for the precipitation time series, the semi-annual cycle is predominant and appears intermittently above the *RedNoise* for the entire study period. It obviously corresponds to the two wet periods characterizing the region's climate (one in spring and the other in autumn), whereas the summer and winter months are associated with dry weather. An interesting finding revealed by the cross-wavelet spectra is that there is a stronger correlation between the NAOi and precipitation on the semi-annual scale, whereas for the WeMOi and precipitation, there is a correlation in the cone of influence in the low-frequency 12–20 year scale. This behaviour could be explained by the fact that the NAO-driven climate phenomenon governs precipitation in the region on the semi-annual and annual scales, whereas components with longer cycles are conditioned by events occurring in the Mediterranean.

The long cycles and the corresponding lags, such as the ones detected between the teleconnection indices and precipitation time series could be explained by their long-term behaviour and fluctuation, related to prolonged negative and positive phases. These findings are in line with the conclusions drawn by Trigo at al. (2004) who points out that the impact of NAO on Iberian Peninsula's precipitation and river flows is irregular, presenting a high inter-decadal variability. They also coincide with the regionalisation made by Martin-Vide & Lopez-Bustins (2006), with the application of only linear correlation analysis between time series of NAOi, WeMOi and precipitation gauges across the entire Iberian Peninsula. These authors defined three areas: (1) a large central and south-western area, negatively well correlated with the NAO; (2) the eastern facade, with a negative correlation with the WeMO and (3) the eastern Cantabrian facade, positively correlated with the WeMO. It is worth noting that our study area is just on the edge where the two climatic influences take place (areas 1 and 2). The frequency scale of around 4–5 years in the precipitation time series of the Southern Iberian Peninsula and North Africa found by Andreo et al. (2006) and Ouachani et al. (2011) has also been detected in our research. The correlation between precipitation and the large-scale teleconnection patterns on that scale is detectable in small windows, which vary over time and do not overlap. This could be due to the fact that the influence of the two large climate patterns alternates over the study region on different time and frequency scales. The temporal variations and the phase differences between the precipitation and the teleconnection indices, representing the atmospheric circulation patterns, are driven by the studied area climate conditions, imposed by its geographical position on the Iberian high plain. The plain acts as air mass barrier for the fronts originated both in the Atlantic Ocean and the Mediterranean Sea. The long-term variation of the atmospheric anomalies may create a delayed influence on the precipitation.

An important aspect in the management and planning of water resources in semi-arid climates with intensive groundwater use (such as that of the MOA) is to minimize the environmental, economic, and social impacts of possible droughts. To this end, the JRB authorities drew up special drought plans (article 27.1 of Law 10/2001). These authorities have well-established indicators and indices to detect drought episodes to establish appropriate management measures (MMA 2007). In addition, special attention has been given in recent years to improving and analysing in detail these status indices and indicators of drought (see a summary in Pedro-Monzonís et al., 2015 and Ortega-Gomez et al., 2018). However, establishing predominant cycles at different frequency scales and localizing the lag-occurrence of the hydrogeological events (i.e. droughts) in the time domain can be of great use to take preventive measures.

Indeed, periodic drought reports from the river basin authorities (CHJ 2005) assert that the uncertainties arising from climate change studies require the inclusion of appropriate changes both in the future analyses of drought conditions and in the corrective measures to be taken. These analyses should take into account not only the frequency but also the intensity of climatological events. More specifically, these documents (CHJ 2005, 2010) propose monthly reports be prepared of the hydro-meteorological status of the basin and quarterly forecasts (deterministic and probabilistic) of the possible evolution of the JRB.

7. Conclusions

The novelty of this work consist in the application of wavelet analysis to a time series of aquifer-river interactions, obtained through numerical modelling, and correlating it to the large climatic patterns and locally measured precipitation as main source of aquifer recharge. This study provides a significant contribution by establishing more precise ways to define plan cycles in complex and intensively exploited hydrological systems, based on a better understanding of the relationships existing between hydrogeological and atmospheric systems, observed climatic and modelled hydrogeological variables. The findings reported here could be applied in decision-making in order to define specific water management measures such as locating in time the occurrence of different hydrological events with a very long return period that are characterized by their intensity. Furthermore, this approach can be extrapolated independently of the geographical location of the hydrogeological system, the basin size, and the climate region.

The results of this investigation indicate that the correlation between precipitation, as the main source of recharge in the zone, and RAI is conditioned mainly by the NAOi at the semi-annual scale,

with a lag between NAOi and PP of three months. Furthermore, in the statistically significant areas, a lag of another three months is detected between precipitation and RAI, which coincides nicely with the quarterly forecasts proposed by the drought reports. Therefore, on a cumulative basis and before the introduction of potential corrective measures, it is necessary to make hydro-meteorological forecasts not only with a time window (or frame) of three months (e.g. quarterly forecasts adopted by the Júcar River Basin Authorities in line with the cycles detected here at the semi-annual scale), but also with a cumulative six-month forecast cycle as the phase difference between RAI and NAOi indicates at the annual scale. On the other hand, low-frequency cycles found in both the RAI-NAO and PP-RAI relations robustly confirm the suitability of performing the planning process through six-year cycles as suggested by the Water Framework Directive.

In summary, wavelet analysis between measured PP and the RAI, and the large teleconnection patterns (NAOi, WeMOi), provides a better understanding of climate processes and their drivers on a regional scale. This study demonstrates the effectiveness of wavelet analysis to characterize climate variability and its connection with hydrogeological systems under anthropogenic pressures, with complex relations between groundwater and surface water bodies. The wavelet analysis applied here allows the occurrence of different hydrological events with a long return period (characterized by their intensity) to be localized in time, thereby expanding our understanding of how large climate patterns and the intensive exploitation of groundwater affects regionally available water resources.

So far, the main obstacle to implementation of this type of tool in water planning has been its novel nature in this field. Nevertheless, both existing studies (view literature in this article) and our own findings show that its application can be successfully used to: (a) decompose hydrogeological time series, extracting climate and anthropogenic components that appear with certain frequencies located primarily in time, before their use in modelling approaches, and (b) establish the intensity/occurrence of hydro-climatological events, and their statistical correlation, that can affect water management.

References

Andreo B, Jiménez P, Durán J, Carrasco F, Vadillo I, Mangin A. 2006. Climatic and hydrological variations during the last 117–166 years in the south of the Iberian Peninsula, from spectral and correlation analyses and continuous wavelet analyses. *Journal of Hydrology* **324** (1-4): 24–39 DOI: 10.1016/j.jhydrol.2005.09.010

Boggess A, Narcowich FJ. 2009. *A first course in wavelets with Fourier analysis*. John Wiley & Sons: Hoboken, NJ.

Butler JJ, Whittemore DO, Wilson BB, Bohling GC. 2018. Sustainability of aquifers supporting irrigated agriculture: a case study of the High Plains aquifer in Kansas. *Water International* **43** (6): 815–828 DOI: 10.1080/02508060.2018.1515566

Cassiraga E, Sanz D, Castaño S, Álvarez O, Sahuquillo A. 2013. Modelo de flujo subterráneo de los acuíferos de la Mancha Oriental y sus relaciones con el río Júcar [Groundwater model flow of the Mancha Oriental Aquifer and their relations with the Júcar River]. Unpublished report (pp 77). *Confederación Hidrográfica del Júcar.*

Castaño S, Sanz D, Gómez-Alday JJ. 2013. Sensitivity of a Groundwater Flow Model to Both Climatic Variations and Management Scenarios in a Semi-arid Region of SE Spain. *Water Resources Management* **27** (7): 2089–2101 DOI: 10.1007/s11269-013-0277-4

Charlier J-B, Ladouche B, Maréchal J-C. 2015. Identifying the impact of climate and anthropic pressures on karst aquifers using wavelet analysis. *Journal of Hydrology* **523**: 610–623 DOI: 10.1016/j.jhydrol.2015.02.003

Commission of the European Communities (CEC) 2000. Directive of the European Parliament and of the Council establishing a framework for Community action in the field of water policy: Joint text approved by the Conciliation Committee. 1997/0067(COD) C5-0347/00

CHJ. 2005. Protocol for action in situations of alert and eventual drought (in Spanish). https://www.chj.es/es-es/medioambiente/gestionsequia/Documents/Plan%20Especial%20Alerta%20y%20Eventual%20Sequia/Protocolo_CHJ_dic2005_JG.pdf

CHJ. 2010. Post-drought report Paragraph 10 PES (in Spanish). https://www.chj.es/es-es/medioambiente/gestionsequia/Documents/Informes%20Seguimiento/INFORME_POST_SEQUIA_2010.pdf

CHJ. 2015. Júcar River Basin Management Plan 2015–2021 (in Spanish). Júcar River Basin Authority (Demarcación hidrográfica del Júcar).Confederación Hidrográfica del Júcar. Ministry of the Environment, Madrid.

Daubechies I. 1992. Ten lectures on wavelets (Vol. 61). Siam

Grinsted A, Moore JC, Jevrejeva S. 2004. Application of the cross wavelet transform and wavelet coherence to geophysical time series. *Nonlinear Processes in Geophysics* **11** (5/6): 561–566 DOI: 10.5194/npg-11-561-2004

Gómez-Martínez G, Pérez-Martín MA, Estrela-Monreal T, Del-Amo P. 2018. North Atlantic Oscillation as a Cause of the Hydrological Changes in the Mediterranean (Júcar River, Spain). *Water Resources Management* **32** (8): 2717–2734 DOI: 10.1007/s11269-018-1954-0

Fleckenstein JH, Niswonger RG, Fogg GE. 2006. River-Aquifer Interactions, Geologic Heterogeneity, and Low-Flow Management. *Ground Water* **44** (6 Understanding): 837–852 DOI: 10.1111/j.1745-6584.2006.00190.x

Harbaugh AW 2005. MODFLOW-2005, the US Geological Survey modular ground-water model: the ground-water flow process (pp. 6-A16). Reston, VA: US Department of the Interior, US Geological Survey.

Holman IP, Rivas-Casado M, Bloomfield JP, Gurdak JJ. 2011. Identifying non-stationary groundwater level response to North Atlantic ocean-atmosphere teleconnection patterns using wavelet coherence. *Hydrogeology Journal* **19** (6): 1269–1278 DOI: 10.1007/s10040-011-0755-9

Hurrell JW. 1995. Decadal Trends in the North Atlantic Oscillation: Regional Temperatures and Precipitation. *Science* **269** (5224): 676–679 DOI: 10.1126/science.269.5224.676

Hurrell JW, Kushnir Y, Ottersen G, Visbeck M. 2003. Preface. *The North Atlantic Oscillation: Climatic Significance and Environmental Impact Geophysical Monograph Series*: vii-viii DOI: 10.1029/gm134p0vii

Jones P, Davies T, Lister D, Slonosky V, Jónsson T, Bärring L, Jönsson P, Maheras P, Kolyva-Machera F, Barriendos M, et al. 1999. Monthly mean pressure reconstructions for Europe for the 1780–1995 period. *International Journal of Climatology* **19** (4): 347–364 DOI: 10.1002/(sici)1097-0088(19990330)19:4<347::aid-joc363>3.0.co;2-s

Jones PD, Jonsson T, Wheeler D. 1997. Extension to the North Atlantic oscillation using early instrumental pressure observations from Gibraltar and south-west Iceland. *International Journal of Climatology* **17** (13): 1433–1450 DOI: 10.1002/(sici)1097-0088(19971115)17:13<1433::aid-joc203>3.0.co;2-p

Komasi M, Sharghi S. 2019. Recognizing factors affecting decline in groundwater level using wavelet-entropy measure (case study: Silakhor plain aquifer). *Journal of Hydroinformatics* **21** (3): 510–522 DOI: 10.2166/hydro.2019.111

Labat D, Ababou R, Mangin A. 2001. Introduction of Wavelet Analyses to Rainfall/Runoffs Relationship for a Karstic Basin: The Case of Licq-Atherey Karstic System (France). *Ground Water* **39** (4): 605–615 DOI: 10.1111/j.1745-6584.2001.tb02348.x

López J, Frances F. 2010. Influence of the North Atlantic Oscillation and the western Mediterranean oscillation in the maximum flow events in Spain. *International workshop advances in statistical hydrology*.

Lopez-Bustins J-A, Martin-Vide J, Sanchez-Lorenzo A. 2008. Iberia winter rainfall trends based upon changes in teleconnection and circulation patterns. *Global and Planetary Change* **63** (2-3): 171–176 DOI: 10.1016/j.gloplacha.2007.09.002

Maraun D, Kurths J. 2004. Cross wavelet analysis: significance testing and pitfalls. *Nonlinear Processes in Geophysics* **11** (4): 505–514 DOI: 10.5194/npg-11-505-2004

Markovic D, Koch M. 2013. Long-term variations and temporal scaling of hydroclimatic time series with focus on the German part of the Elbe River Basin. *Hydrological Processes* **28** (4): 2202–2211 DOI: 10.1002/hyp.9783

Martin-Vide J, Lopez-Bustins J-A. 2006. The Western Mediterranean Oscillation and rainfall in the Iberian Peninsula. *International Journal of Climatology* **26** (11): 1455–1475 DOI: 10.1002/joc.1388

Milly PCD, Betancourt J, Falkenmark M, Hirsch RM, Kundzewicz ZW, Lettenmaier DP, Stouffer RJ. 2008. Stationarity Is Dead: Whither Water Management? *Science* **319** (5863): 573–574 DOI: 10.1126/science.1151915

MMA Ministerio de Medio Ambiente. Orden MAM/698/2007, de 21 de Marzo, Por la Que se Aprueban los Planes Especiales de Actuación en Situaciones de Alerta y Eventual Sequía en los Ámbitos de los Planes Hidrológicos de Cuencas Intercomunitarias. Boletín Oficial del Estado. Available at: https://www.boe.es/eli/es/o/2007/03/21/mam698

Mukherjee A, Saha D, Harvey CF, Taylor RG, Ahmed KM, Bhanja SN. 2015. Groundwater systems of the Indian Sub-Continent. *Journal of Hydrology: Regional Studies* **4**: 1–14 DOI: 10.1016/j.ejrh.2015.03.005

Ortega-Gómez T, Pérez-Martín MA, Estrela T. 2018. Improvement of the drought indicators system in the Júcar River Basin, Spain. *Science of The Total Environment* **610-611**: 276–290 DOI: 10.1016/j.scitotenv.2017.07.250

Osborn TJ. 2006. Recent variations in the winter North Atlantic Oscillation. *Weather* **61** (12): 353–355 DOI: 10.1256/wea.190.06

Osman YZ, Bruen MP. 2002. Modelling stream–aquifer seepage in an alluvial aquifer: an improved loosing-stream package for MODFLOW. *Journal of Hydrology* **264** (1-4): 69–86 DOI: 10.1016/s0022-1694(02)00067-7

Ouachani R, Bargaoui Z, Ouarda T. 2011. Power of teleconnection patterns on precipitation and streamflow variability of upper Medjerda Basin. *International Journal of Climatology* **33** (1): 58–76 DOI: 10.1002/joc.3407

Pedro-Monzonís M, Solera A, Ferrer J, Estrela T, Paredes-Arquiola J. 2015. A review of water scarcity and drought indexes in water resources planning and management. *Journal of Hydrology* **527**: 482–493 DOI: 10.1016/j.jhydrol.2015.05.003

Puri S, Aureli A. 2009. Atlas of Transboundary Aquifers: Global maps, regional cooperation and local inventories. *ISARM Program.*

Salerno F, Tartari G. 2009. A coupled approach of surface hydrological modelling and Wavelet Analysis for understanding the baseflow components of river discharge in karst environments. *Journal of Hydrology* **376** (1-2): 295–306 DOI: 10.1016/j.jhydrol.2009.07.042

Sang Y-F, Wang Z, Liu C. 2012. Discrete wavelet-based trend identification in hydrologic time series. *Hydrological Processes* **27** (14): 2021–2031 DOI: 10.1002/hyp.9356

Sanz D. 2005. *Contribución a la caracterización geométrica de las unidades hidrogeológicas que integran el sistema de acuíferos de la Mancha Oriental (Contribution to the geometric characterization of the hydrogeological units of the La Mancha Oriental aquifer system),* Memoria para optar al grado de doctor (PhD thesis). Universidad Complutense de Madrid, Facultad de Ciencias Geológicas, Departamento de Geodinámica. ISBN: 84-669-2802-2.

Sanz D, Gómez-Alday JJ, Castaño S, Moratalla A, Heras JDL, Martínez-Alfaro PE. 2009. Hydrostratigraphic framework and hydrogeological behaviour of the Mancha Oriental System (SE Spain). *Hydrogeology Journal* **17** (6): 1375–1391 DOI: 10.1007/s10040-009-0446-y

Sanz D, Castaño S, Cassiraga E, Sahuquillo A, Gómez-Alday JJ, Peña S, Calera A. 2011. Modeling aquifer–river interactions under the influence of groundwater abstraction in the Mancha Oriental System (SE Spain). *Hydrogeology Journal* **19** (2): 475–487 DOI: 10.1007/s10040-010-0694-x

Sanz D, Vos J, Rambags F, Hoogesteger J, Cassiraga E, Gómez-Alday JJ. 2018. The social construction and consequences of groundwater modelling: insight from the Mancha Oriental aquifer, Spain. *International Journal of Water Resources Development* **35** (5): 808–829 DOI: 10.1080/07900627.2018.1495619

Torrence C, Compo GP. 1998. A Practical Guide to Wavelet Analysis. *Bulletin of the American Meteorological Society* **79** (1): 61–78 DOI: 10.1175/1520-0477(1998)079<0061:apgtwa>2.0.co;2

Trigo RM, Pozo-Vázquez D, Osborn TJ, Castro-Díez Y, Gámiz-Fortis S, Esteban-Parra MJ. 2004. North Atlantic oscillation influence on precipitation, river flow and water resources in the Iberian Peninsula. *International Journal of Climatology* **24** (8): 925–944 DOI: 10.1002/joc.1048

Winston RB. 2009. ModelMuse - A Graphical User Interface for MODFLOW-2005 and PHAST. *Techniques and Methods* DOI: 10.3133/tm6a29

Data Availability Statement

The datasets that support the findings of this study are from different sources and their availability varies. Climate indices data are downloadable from the public domain and for the North Atlantic Oscillation index the data were derived from the following resource: [https://crudata.uea.ac.uk/cru/data/nao/nao.dat], while for the Western Mediterranean Oscillation index the data were obtained from: [http://www.ub.edu/gc/documents/Web_WeMOi.txt].

Restrictions may apply to the availability of the precipitation data and for the purpose of this study the data were received after written request from the State Meteorological Agency of Spain.

The time series data of river-aquifer interactions were obtained with numerical groundwater flow model, using Modflow code. The information is available from the corresponding author upon reasonable request.

Table 1. General description and descriptive statistics of the studied time series for the North Atlantic Oscillation index (NAOi), Western Mediterranean Oscillation index (WeMOi), Precipitation (PP), and River-aquifer interactions (RAI) for the period of 1940–2012.

General description	RAI	Precipitation Stations			NAOi Stations	WeMOi Stations
Location	-	8152 La Gineta	8175 Los Llanos	8178 Instituto	Reykjavik Gibraltar	Padua San Fernando
Latitude	-	39.12°N	38.95°N	39.00°N	64.10°N 36.20°N	45.40°N 36.28°N
Longitude	-	2.00°W	1.86°W	1.86°W	21.90°W 5.40°W	11.48°E 6.12°W
Elevation, m a.s.l.	-	688	702	686	sea level	sea level
Descriptive statistics	RAI hm^3/month		PP mm/month		NAOi dimensionless	WeMOi dimensionless
Mean	-13.70		29.36		0,03	0.12
Maximum/Year	3.42/2001		201.40 / 1996		6.66 / 1947	4.18 / 1912
Minimum/Year	-25.67/1997		0.00 / *		-4.70 / 1996	-4.29 / 2006
Standard deviation	5.81		28.14		1.73	1.20

*The minimum of 0 mm of accumulated precipitation per month is registered in 28 of the 73 studied years (1940–2012).

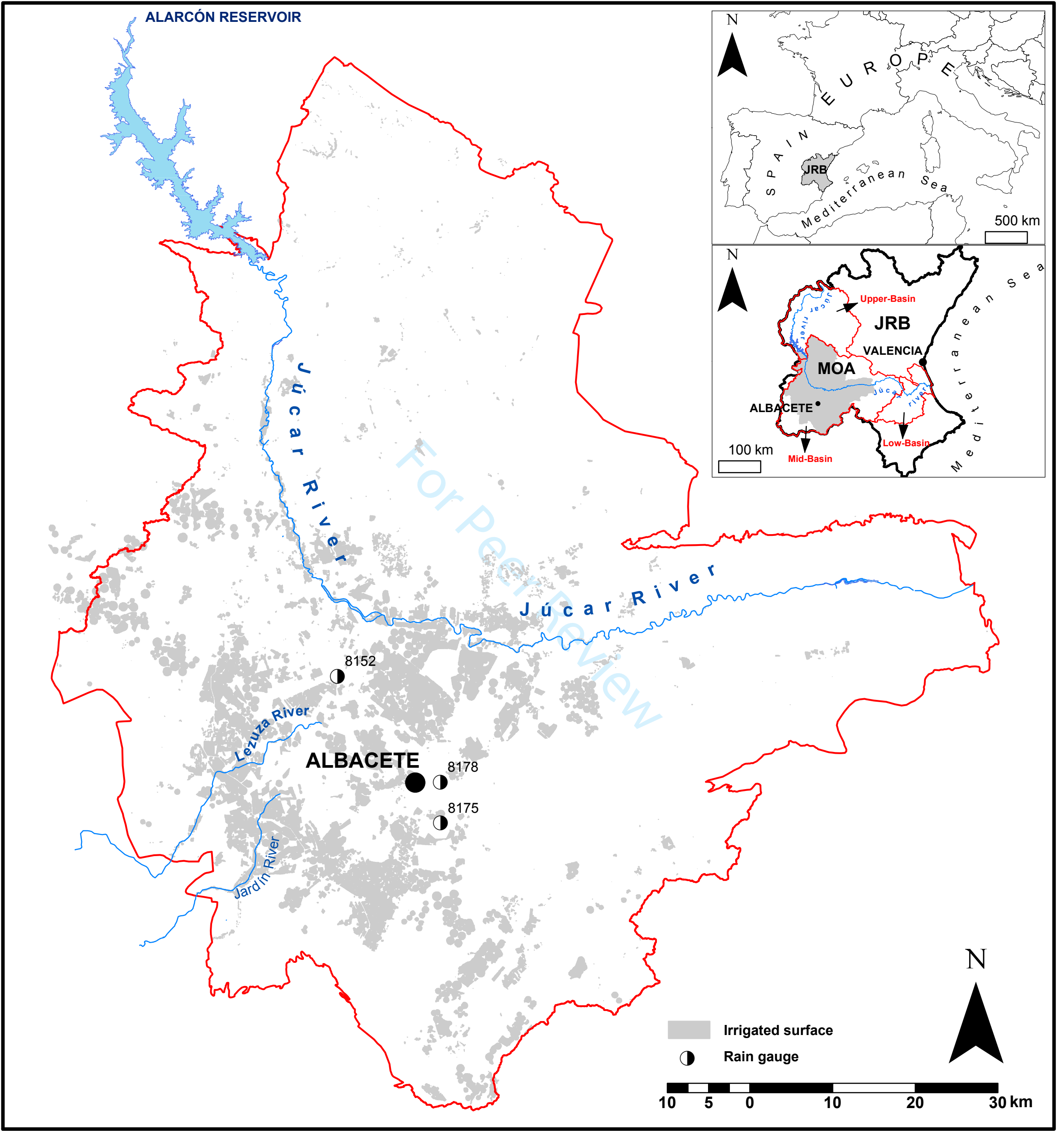

FIGURE 1 Location of the study area. JRB: Júcar River Basin, MOA: Mancha Oriental Aquifer.

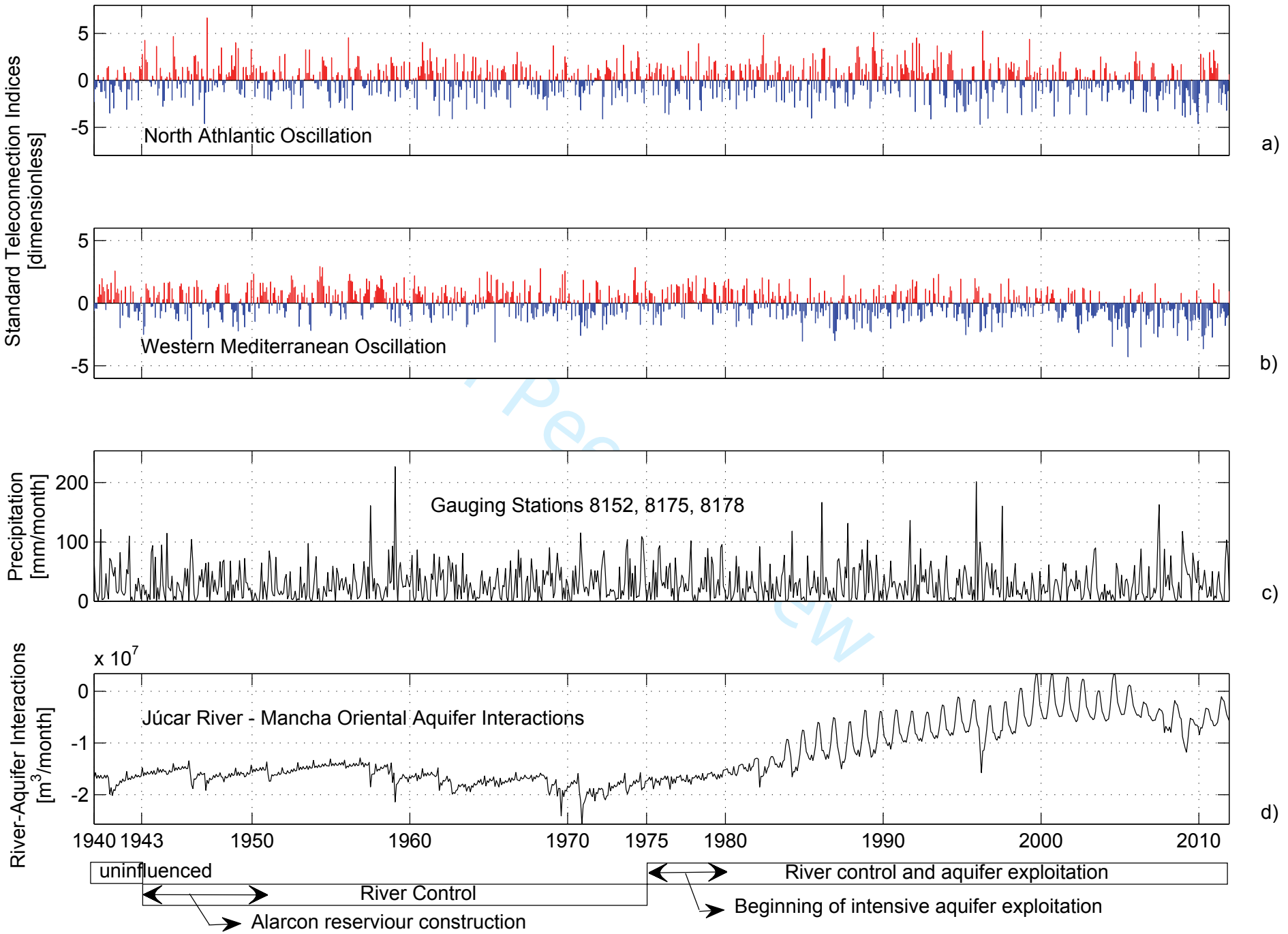

FIGURE 2 Data used, from the top (a) to the bottom (d): (a) NOAi; (b) WeMOi, positive (red) and negative (blue) phases of the standardised seasonal teleconnection indices; (c) Precipitation in the MOA, monthly data gauging stations 8152, 8175, 8178 (see location in Figure 1); (d) River-aquifer interactions (RAI obtained with MODFLOW groundwater flow modelling). Negative values indicate the river is gaining and positive values show the river is losing.

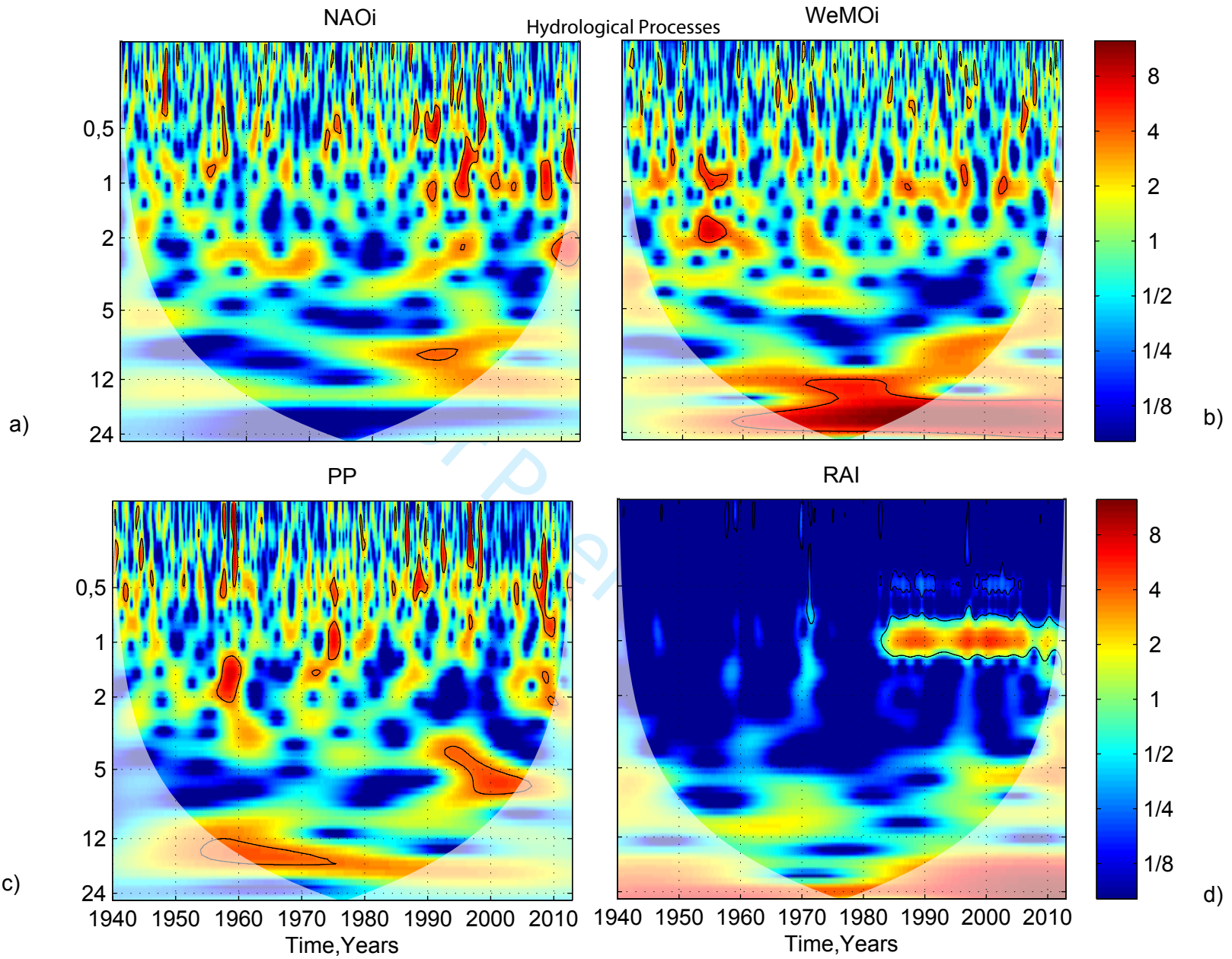

FIGURE 3 Wavelet power spectra of the hydroclimatic time series: (a) North Atlantic Oscillation index (NAOi), (b) Western Mediterranean
Oscillation index (WeMOi), (c) Precipitation in Albacete (PP) and (d) River–aquifer interactions (RAI). The wavelet power at each period is
normalized by the global wavelet spectra (dimensionless). The RGB colour scales indicate the value of the wavelet coefficient. The thick black
outline indicates the 5% significance level against RedNoise. The cone of influence, where edge effects might distort the picture, is shown in a
lighter shade

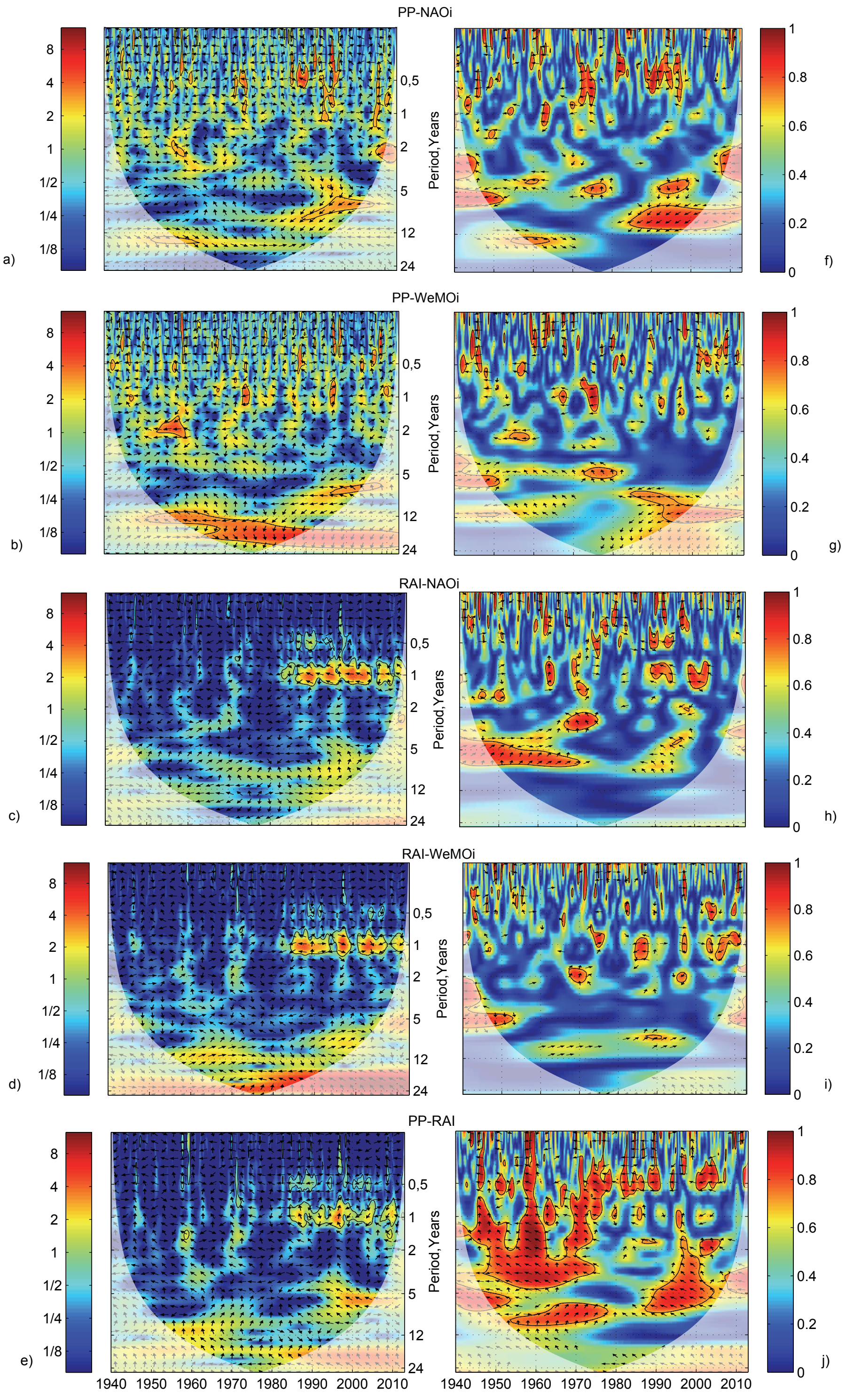

FIGURE 4 Cross-wavelet spectra (a–e) and wavelet coherence (f–j) between PP, RAI, the NAOi and the WeMOi. The first row shows the correlation and the covariation between PP and the NAOi, the second between PP and the WeMOi, the third between RAI and the NAOi, the fourth between RAI and the WeMOi, while the bottom row shows the relations between PP and the RAI. The thick black outline indicates the 5% significance level against RedNoise and the cone of influence where edge effects might occur is shown as a lighter shade.
Phase arrows pointing right means that the two variables are in-phase, left is in antiphase, up/down: 90º lead/lag